

# Quantum Coherence is Preserved in Extremely Dispersive Plasmonic Media

(short title: Plasmons are robust against decoherence)

## Authors

Yury S. Tokpanov<sup>1</sup>, James S. Fakonas<sup>1</sup>, Benjamin Vest<sup>1</sup>, and Harry A. Atwater<sup>1\*</sup>

## Affiliations

<sup>1</sup>Thomas J. Watson Laboratories of Applied Physics, California Institute of Technology, Pasadena, California 91125.

\*Email : haa@caltech.edu

## Abstract

Quantum plasmonics experiments have on multiple occasions reported the observation of quantum coherence of discrete plasmons, which exhibit remarkable preservation of quantum interference visibility, a seemingly surprising feature for systems mixing light and matter with high ohmic losses during propagation. However, most experiments to date used essentially weakly-confined plasmons, which experience limited light-matter hybridization, thus limiting the potential for decoherence. Here, we report quantum coherence of plasmons near the surface plasmon polariton (SPP) resonance frequency, where plasmonic dispersion and confinement is much stronger than in previous experiments. We generated polarization-entangled pairs of photons using spontaneous parametric down conversion and transmitted one of the photons through a plasmonic hole array designed to convert incident single photons into highly-dispersive single SPPs. We find the quality of photon entanglement after the plasmonic channel to be unperturbed by the introduction of a highly dispersive plasmonic element. Our findings provide a lower bound of 100 femtoseconds for the pure dephasing time for dispersive plasmons in gold, and show that even in a highly dispersive regime surface plasmons preserve quantum mechanical correlations, making possible harnessing the power of extreme light confinement for integrated quantum photonics.

## MAIN TEXT

Understanding the quantum nature of light and matter is of central importance for advancing modern technology. For example, one approach to physical realization of a quantum computer is envisioned to be through the use of linear optical components (1), which can be arranged in the form of integrated photonic circuits. Since some of the building block elements for such a scalable quantum photonic system (phase shifters, modulators, directional couplers, etc...) and the coherence and fabrication requirements are very similar to present-day chip-based nanophotonic circuit elements, recent experimental advances (2) has inspired optimism about the technical feasibility of quantum integrated photonic systems, if suitable single-photon sources, memories and detectors can be realized.

One of the important branches of photonics is plasmonics, which enables extreme light confinement utilizing surface plasmon polaritons (SPPs), the quanta of so-called surface plasma waves that are excited on the boundary between a metal and a dielectric (3). SPPs are bosons, so their quantum statistical behavior is expected to be similar to that of photons. By confining electromagnetic energy in small modal volumes, plasmonics allows significantly enhanced light-matter interactions at the nanoscale, and has found interesting applications in classical photonics for sensing (4,5), sub-diffraction limit imaging (6,7), and paving the way towards strong light-matter interactions, by reaching for example strong coupling regimes (8,9). However, light-matter hybridization in SPPs has an important consequence. SPPs are collective excitation of electrons with a mixed electronic and electromagnetic character, while photons in free space are purely electromagnetic excitations, and light propagating through dielectric linear media is described by polaritons, mixing mixing electromagnetic excitation and the motion of bound electrons that do not experience much interactions with the rest of the environment. Through the motion of electrons in the metal SPPs are coupled to matter by many degrees of freedom. One consequence is that SPPs experience propagating losses due to the Ohmic losses of the moving electrons comprised in an SPP. In fully quantum optical picture, light-matter hybridization could be anticipated to make SPPs sensitive to decoherence from dephasing which is often present in systems with Ohmic losses, leading to disappearance of their quantum features such as entanglement.

Recently, several groups have performed plasmonic analogues to landmark quantum optics experiments using SPPs in lieu of single photons, yielding results such as single plasmon interferences (10,11), a plasmonic Hong-Ou-Mandel experiment (12-14) and entanglement experiments (15-17). These successful experiments faced significant plasmonic absorption, manifested as Ohmic losses, but managed to preserve enough of the plasmons to highlight various quantum features of discrete SPPs. However, an apparently surprising result was that most of the results reported very good or excellent preservation of the quantum interference contrast, possibly indicating that pure dephasing processes are much slower than pure absorption. Notably in each of these experiments, despite the fact that the experimental conditions pre-selected and tested the coherence of the ‘surviving’ non-absorbed plasmons, the strong plasmonic absorption observed is the undeniable sign of non-negligible coupling between the particles and their environment. The observation of such coupling is an indication that the degrees of freedom of the plasmons are likely to become entangled with the degrees of freedom of the environment, a description that is commonly used to explain the vanishing of quantum interference features, or in other words, decoherence. This has been verified, for example, in an experiment based on plasmonic waveguides (18). Decoherence is one of the limiting factors for current and future quantum technology. Hence the question of how SPPs lose quantum mechanical coherence and if their quantum properties can be protected over long propagation distances or under strong light-matter interactions is of significant importance.

We note that until now, quantum plasmonics experiments used exclusively plasmons in a regime far from the SPP resonance. In other words, the plasmons exhibited a highly “photon-like” behavior with weak confinement, that intrinsically limits the decoherence processes. Indeed, in the case of photon-like plasmons, we expect the plasmon resonances to have only a weak admixture with the electronic degrees of freedom in the metal, leaving the gateway only ajar to significant coupling and entanglement between the SPPs and the metallic environment. Therefore, in this photon-like regime, one could argue that from the perspective of decoherence processes, some

quantum plasmonics experiments are somewhat analogous to other quantum optics experiments performed with photons all the way and exhibiting no decoherence. That would also mean that plasmonic losses here play a role that is not different from optical losses introduced by beam splitters, stray reflections, or neutral density filters. Thus, there is need to investigate quantum plasmonics in other regimes of plasmon propagation, where the competition between absorption and pure dephasing could result in observable decoherence.

In this paper, we report results of a quantum plasmonics experiment to investigate two ways to affect decoherence processes and the disappearance of quantum entanglement. More precisely, in a series of experiments inspired by (15), we measure the preservation of polarization entanglement between two photons after one photon is converted into a plasmon propagating on a hole array, which is then subsequently reconverted into a photon (19). First, as a warm-up experiment, we modified the geometry of the hole array, using elliptical holes to create different conditions for plasmon polarization, effectively introducing distinguishability between them and thus reducing the quality of the entangled state. This allows us to work first in a linear regime for plasmon dispersion. Secondly, we performed polarization entanglement experiments in plasmonic hole arrays with circular holes but which are designed to be in a highly dispersive regime, i.e. with single plasmons close to the SPP resonance. In this highly dispersive regime, SPPs are tightly confined and have a much stronger interaction with the electronic system (one manifestation of which is larger absorption), which in principle can lead to destruction of quantum correlations. This experiment aims to build a better understanding of the robustness of quantum phenomena in quantum plasmonics.

## Results

In our experimental work, we generate pairs of polarization-entangled photons, propagating along two different paths, and interpose a plasmonic hole array in the path of one of the photons. This photon is thus converted into a plasmon, and the detected signal consists of plasmons reconverted into free-space photons after plasmon propagation over a few hundred nanometers in the hole array (15). The quality of polarization entanglement between both outcoupled photons is measured and is representative of the effects of light-matter interactions during plasmon propagation. Whereas the work reported in (15) probed hole arrays with linear dispersion and circular holes, we investigate: i) first, the influence of hole geometry the quality of entanglement in the linear regime and ii) second, we measure preservation of entanglement between photons when the plasmonic hole array operates in a highly dispersive regime, to probe plasmon decoherence.

**Generation of entangled pairs of particles** As a source of polarization-entangled photons we used type-I spontaneous parametric down-conversion (SPDC), occurring in a pair of nonlinear bismuth borate (BiBO) crystals. They are rotated by  $90^\circ$  with respect to each other and glued together (20) (Fig. 1), so that one crystal has its axis in the horizontal plane and the other one in a vertical plane. The pair of crystals is pumped by a laser diode emitting at 406 nm. The pump photons are linearly polarized at  $45^\circ$  with respect to the nonlinear crystal axis planes, so that type-I SPDC generate pairs of photons at 812 nm that are polarized parallel to either the horizontal direction or the vertical direction with equal probabilities. This setup generates polarization-entangled photons that, before their interaction with the environment  $|E\rangle$  (plasmonic sample), can be described by the superposition state:

$$|\psi\rangle_{initial} = \frac{1}{\sqrt{2}} [e^{i\Delta\varphi_c} |H, H\rangle + |V, V\rangle] \otimes |E\rangle \quad (1)$$

where  $\Delta\varphi_c$  is a phase delay between the two polarizations, due to the birefringence of BiBO crystals.

The twin photons propagate in a horizontal plane, along the opposite edges of a cone whose apex angle is  $6^\circ$ . Each photon is focused towards a polarizer and a single-photon avalanche diode (SPAD). The detection of a photon by one of the SPADs is a projective measurement of its polarization state. A plasmonic hole array can be placed along one of the propagation paths, thus forcing one of the photon to be temporarily converted into a plasmon before eventually being detected.

In our experiment, in order to correctly estimate the influence of pure dephasing processes, we retain only coincident counts between the two SPADs, i.e. we consider only the case when both photons register counts at the detectors. In other words, when the hole array is in place, we do not record events in which a plasmon has decayed through inelastic interactions with the electronic system – this is a well-understood mechanism for decoherence. On the contrary, we collect only photons from events in which the plasmon has survived. Such events, in principle, can be affected by elastic interactions or the inner structure of the plasmon quasiparticle.

In the general case, after propagation of the quantum entangled state and before applying any projective measurement, we can consider that the light has become entangled with the environment, and we can write

$$|\psi\rangle_{final} = \frac{1}{\sqrt{|h|^2+|v|^2}} [he^{i\Delta\varphi_c}|H, H\rangle \otimes |E_H\rangle + v|V, V\rangle \otimes |E_V\rangle] \quad (2)$$

where  $h$  and  $v$  – are complex amplitude transmission coefficients for horizontal polarization  $|H\rangle$  and vertical polarizations  $|V\rangle$  respectively;  $|E_H\rangle$  and  $|E_V\rangle$  are environmental states, entangled with horizontal and vertical polarizations respectively.

By tracing over environmental states one can obtain a reduced density matrix, from which a probability of a coincidence count can be computed:

$$\begin{aligned} P_{cc}(\alpha, \beta) &= \langle \alpha, \beta | \hat{\rho}_{reduced} | \alpha, \beta \rangle = \\ &= \frac{1}{1+\frac{|v|^2}{|h|^2}} \left[ \sin^2 \alpha \sin^2 \beta + \frac{|v|^2}{|h|^2} \cos^2 \alpha \cos^2 \beta + \right. \\ &\left. \frac{1}{2} \sin(2\alpha) \sin(2\beta) \frac{|v|}{|h|} |\langle E_V | E_H \rangle| \cos(\varphi_E + \Delta\varphi + \Delta\varphi_c) \right] \quad (3) \end{aligned}$$

where  $\frac{v}{h} = \frac{|v|}{|h|} e^{-i\Delta\varphi}$ ,  $\Delta\varphi$  being the phase difference between the complex amplitude  $h$  and  $v$ ,  $\langle E_V | E_H \rangle = |\langle E_V | E_H \rangle| e^{i\varphi_E}$ ,  $\varphi_E$  being the phase difference between the two environmental states, and  $\alpha$  and  $\beta$  are the polarizer directions with respect to the vertical axis.

The first two terms can be obtained by classical analysis, whereas the last term is the so-called quantum interference term, which represents quantum mechanical nature of our system. Indeed, Eq. (2) describes a superposition state. The quantum interference term can be understood as the interference amplitude between the two terms of the superposition state when projective measurements are carried out on the two-particle state. The amplitude of this term depends on several factors. It depends sinusoidally on the polarizers directions, and is maximum for appropriate choices of the polarizer directions verifying  $|\sin(2\alpha) \sin(2\beta)| = 1$ . This corresponds

to the situation where the photonic parts of both terms in Eq. (2) are projected on a common state with equal amplitude. The amplitude of the quantum term is governed by the ratio  $\frac{v}{h} = \frac{|v|}{|h|} e^{-i\Delta\varphi}$ , which includes all perturbations inherent to the setup that affect the balance between the horizontal and the vertical polarization. Finally, we note here that the magnitude of quantum interference is also determined by the overlap between different environment states  $\langle E_V|E_H\rangle = |\langle E_V|E_H\rangle| e^{i\varphi_E}$ , which represents quantum mechanical decoherence. The presence of  $\Delta\varphi_c$  in the last cosine factor of the quantum interference term shows that, in order to make judgements about quantum decoherence, one has to take a great care in eliminating or measuring phase differences between different polarizations. This can be done by inserting another birefringent element in the setup that will compensate the phase difference between the two polarizations. Optimization and alignment of our SPDC source included tweaking of a  $\lambda/4$  plate (Fig. 1), which allowed us to experimentally eliminate  $\Delta\varphi_c$  in equation (3).

Consider  $h = v$ , which represents equal probability of detecting horizontally or vertically polarized pairs of photons. In the case of absolute coherence  $\langle E_V|E_H\rangle = 1$  ( $E_V = E_H$ ) we get a rather simple expression  $P_{cc}(\alpha, \beta) = \frac{1}{2} \cos^2(\alpha - \beta)$ . There is no entanglement between the photon state and the environment. This ensures the preservation of polarization entanglement between photons. By contrast, in the case of total decoherence  $\langle E_V|E_H\rangle = 0$  we get a straight line  $P_{cc}(\alpha, \beta = 45^\circ) = \frac{1}{4}$  regardless of  $\alpha$  (if  $\beta$  is kept fixed at  $45^\circ$ ). Both terms of the superposition in (2) are now incoherent, and quantum interferences vanish. The measured state can be considered as a statistical mixture of the two states  $|H, H\rangle$  and  $|V, V\rangle$  in equal proportions.

These considerations suggest a measure of quality of the entanglement, visibility, which we define simply as the visibility of the cosine curve described by  $P_{cc}(\alpha, \beta = 45^\circ)$  for the case when we keep polarizer  $\beta$  fixed at  $45^\circ$  (both polarizations contribute to the measurement)  $V = \frac{P_{cc}^{max} - P_{cc}^{min}}{P_{cc}^{max} + P_{cc}^{min}}$ , where  $P_{cc}^{min}$  is the minimum probability of coincidence count (rate in an experiment) and  $P_{cc}^{max}$  is the maximum rate. For  $v = h$  the visibility is equal to  $V = |\langle E_V|E_H\rangle| \cos(\varphi_E + \Delta\varphi + \Delta\varphi_c)$ . From the above analysis we get that  $V = 100\%$  for fully entangled (quantum) light ( $\langle E_V|E_H\rangle = 1$ ), and  $V = 0\%$  for a pure statistical mixture of polarizations (classical light,  $\langle E_V|E_H\rangle = 0$ ). Note, that visibility of a cosine  $P_{cc}(\alpha, \beta = 45^\circ)$  is identical to the visibility of the cosine  $P_{cc}(\alpha, \beta = 135^\circ)$ , hence we can use either one of them, or use one versus another to validate the correctness of the measurement.

In addition to that, we performed Bell's inequalities violation measurements, where we use Bell's inequalities in so-called CHSH form (21, 22). We performed 16-point measurements in order to calculate Bell's parameter  $S$ , comparing our experimental measurement with the best possible prediction of any classical local hidden variable theory (LHVT).  $S > 2$  indicates the impossibility of the explanation by any LHVT.

We characterized our SPDC source (Fig. 2) without plasmonic samples, measuring visibility on the order of  $V = 99\% \pm 1\%$  and  $S = 2.81 \pm 0.02$ , which is just a standard deviation away from the maximal theoretical value  $S_{max} = 2\sqrt{2} \approx 2.83$ . From this, we conclude that we have high quality pairs of entangled photons. In the next sections, we investigate the influence of the insertion of a plasmonic hole array on the quality of entanglement between photons, as defined by the previous measurement procedures.

**Elliptical hole array in the linear regime** The different structures used for the hole arrays have been numerically designed (Fig. 3) and fabricated in a clean room environment. To study geometrical effects, we used a plasmonic array of elliptical holes milled through a 200nm thick layer of gold deposited on a glass substrate (see Fig 3 (A)), by using a focused ion beam with purposely-introduced astigmatism. The dispersion relation of the gold-glass interface was computed from an analytical modal dispersion model. A first choice for the hole dimensions and the array periodicity was made after numerical simulations of the structure designed to enhance extraordinary transmission at 812 nm – the wavelength of our down-converted photons. The sample we used had a size 1mm x 1mm with and was fabricated in a clean room environment. Its transmission was sufficient enough to detect satisfying level of signal. The hole shape in these arrays is close to elliptical, with axes equal to 240nm and 190nm (see Fig 4.(A)). The difference between those two dimensions makes the optical transmission of this sample polarization-dependent (Fig. 4(B)). This sample has linear SPP dispersion (fig. 1c), so that we could focus on hole geometry effects only in this experiment.

First, we performed a measurement using entangled light (Fig. 4(C)) (rotating a sample in such a way that hole array eigenmodes directions were along the vertical and horizontal polarizations). The transmission of the first channel (considered as an influence of the environment on the system) being now polarization dependent, we expect the two terms of the state in Eq. (2) to be differently affected by the insertion of the plasmonic array, and thus a reduction of the visibility. In both of them we found the visibility of curves, corresponding to the mixture of eigenmodes ( $\beta = 45^\circ$  and  $\beta = 135^\circ$  on Fig. 4(C)) of hole array, to be  $V = 86\% \pm 5\%$ .

However, we need to determine to what extent this reduction is caused by the quantum mechanical decoherence (through a decrease of the overlap factor  $V = |\langle E_V | E_H \rangle| \cos(\varphi_E + \Delta\varphi + \Delta\varphi_c)$ ) or by the modification of the complex transmission ratio  $h/v$ , which is a purely classical effect. In order to do so, we performed a control experiment using classical light, in which we generated just unentangled polarized photon pairs, either in the pure  $|H, H\rangle$  state, or in the pure  $|V, V\rangle$  state.(Fig. 4(D)). To record Fig. 4(D) we first fixed the hole array at exactly the same rotation as used in Fig. 4(C) and transmitted horizontal and then vertical polarizations (H0, V0 curves on Fig.4(D) correspond to  $\beta=0^\circ$  and  $\beta=90^\circ$  on Fig. 4(C)). The amplitude ratio between the two sine curves is an indication of the ratio of the transmission amplitude of horizontal and vertical polarization through the hole array  $|h/v|$ . Then we rotated the hole array by  $45^\circ$  and repeated the measurement (H45, V45 curves on Fig.4(D)) correspond to  $\beta=45^\circ$  and  $\beta=135^\circ$  on Fig. 4(C)). In this configuration, the hole array behaves as a birefringent plate whose axis are at  $45^\circ$  with respect to the polarization of the incident photon. The dephasing and the transmission ratio between the two eigenpolarizations can be related to the azimuth and the ellipticity of the output polarization of the photon. From the measurement with classical light and by fitting the different plots of Fig. 4(D), we determined  $\frac{|h|}{|v|} = 5.2 \pm 0.3$  and  $\Delta\varphi = 48^\circ \pm 4^\circ$ . Substituting these values to Eq.(3) and fitting (3) to curves on Fig. 4 (C) gives  $|\langle E_V | E_H \rangle| = 1.0 \pm 0.1$  and,  $\Delta\varphi_E = 1^\circ \pm 4^\circ$  so that within experimental error we did not detect quantum mechanical decoherence.

Breaking the symmetry of the hole shape introduces distinguishability between the eigen polarizations of the problem and degrade the visibility of interferences. However, the reported decrease in visibility is strictly analogous to the classical situation of an unbalanced interferometer,

where two waves of non-equal amplitudes interfere, leading to non-optimal fringe contrast. The reduction of visibility is, in this case, a purely classical effect.

**Hole array with nonlinear dispersion** In this section, we investigate the same polarization entanglement processes using single SPPs that propagate in a hole array, but this time in a regime of highly nonlinear dispersion, far from the light line, in an attempt to reveal effects of pure dephasing on decoherence through a decrease of entanglement visibility. In the highly dispersive regime, the quasiparticle confinement at the metal dielectric interface is much stronger due to the reduction in the plasmon wavelength. In other words, the plasmons excitation wavefunction has a much larger overlap with the electronic degrees of freedom in the metal. As a consequence, plasmons in the highly dispersive regime have a generally higher rate of interaction with the electronic system than in the case of materials with linear dispersion. Hence, in addition to shorter total decoherence time, one can expect a shorter pure dephasing time  $T_2^*$  (which is the relevant time scale probed by our experiment). On the other hand, the group velocity of highly dispersive plasmons is an order of magnitude smaller than for plasmons in the photon-like regime ( $0.05c$  versus  $0.59c$ , where  $c$  is the speed of light in vacuum), so that these plasmons propagate for a longer time  $t_p$  (even if the propagation distances are the same). Therefore, for comparable experiments (i.e. similar propagation distances), strongly-confined plasmons are expected to experience greater decoherence thus exhibit weaker quantum interference than photon-like plasmons.

In order to probe the highly dispersive regime, we use plasmons at the interface between gold and amorphous silicon. Amorphous silicon has a higher dielectric constant than glass, moving the SPP resonance frequency close to the frequency of entangled photons (see Fig. 3(B)). The use of a higher index material leads both the stronger confinement of the plasmons (with a 6-fold increase of the plasmon wave vector) and a 12-fold reduction of their group velocity.

We used a 2mm by 2mm hole array configured in a three-layer structure (50nm of amorphous silicon – 100nm of gold – 50nm of amorphous silicon) and a periodicity  $P=850\text{nm}$  (fig. 5(A)), following from optimization procedure performed with Lumerical. We find a plasmon-enhanced transmission peak at the desired 812nm wavelength (fig. 5(B)). In this hole array SPPs excited on the top and bottom gold surfaces are uncoupled and have the same dispersion. We performed additional analysis and confirmed that the fabricated structure correctly reproduces the initially simulated behavior and operates in the non-linear dispersion regime, far from the light line (See Supplementary Information).

Thanks to the larger size of the sample we were able to collect a larger portion of transmitted light and hence improve our statistics (fig. 5(C)). We recorded a visibility of  $V = 98\% \pm 2\%$  and Bell's number  $S = 2.83 \pm 0.04$ : this measurement implies that even in the highly-dispersive regime, the entanglement is perfectly preserved and no quantitative signs of pure dephasing could be detected. Through numerical computation of the dispersion relation, we can estimate the propagation time to be on the order of  $t_p \sim \frac{1.2\mu\text{m}}{0.05c} \sim 80\text{fs}$ , based on the distance between two diagonally separated holes. This time is much longer than the value of total dephasing time  $T_2 = 2 T_1 = 20\text{fs}$ , that can be estimated from the absorption length in our sample (less than 200nm, in agreement with literature reported values (23)). Another approach towards an estimation of the propagation time based on an approximate lorentzian fit of the resonance experienced by the plasmons gives a similar time. We therefore conclude that in our system, pure dephasing is a remarkably slow process compared to absorption, and the order of magnitude of the lower bound of the dephasing

time can be estimated to be 100 fs, which is similar to the value reported in (15). We note however that this time could be in practice much higher, as our experiment remarkably reports no quantitative trace of quantum decoherence. Performing the same experiment in an even more highly dispersive regime could hypothetically allow us to make decoherence process eventually visible at some extent. This would make the degradation of the fringes visibility capable of being modeled, one of the parameters of such a model being the pure dephasing time, that could be more precisely estimated. The design of such an experiment is however fundamentally limited by the high level of absorption that coexists with the enhancement of light-matter interactions. It dramatically reduces the signal level at the output of the plasmonic path progressively to almost zero.

## **Discussion**

We have examined the influence of plasmon dispersion on the quantum decoherence properties of surface plasmons. Neither excitation of highly-dispersive plasmons, nor altering the hole array geometry resulted in the reduction of the quality of a single-particle quantum state for transmitted light. Plasmons excited in highly dispersive hole arrays are found to preserve quantum mechanical correlations, even in the presence of extreme dispersion near the plasmon resonance and strong absorption. Moreover, the focus of our measurements is on the elastic dephasing processes, which consideration is commonly neglected in quantum optics modeling due to the supposed insignificance. Our findings provide experimental proof for such an assumption, and also emphasize the difference between decay and decoherence. Thus, we conclude that despite being lossy, plasmonic structure may find applications in the realms of quantum technology, where the power of extreme light confinement can be effectively leveraged.

## **Materials and Methods**

**Sample numerical design and fabrication.** The simulations have been performed with Lumerical, using the optical constants of (24) for amorphous silicon and (25) for gold. The elliptical hole array was fabricated by depositing about 200nm of gold on a glass substrate in a e-beam evaporator (Angstrom Engineering). Holes were milled by Focused Ion Beam (Versa 3D), using the astigmatism of the beam to shape the holes. The high-dispersion hole array was made by depositing several layers of amorphous silicon in a sputterer (ATC Orion by AJA International), a layer of gold in the e-beam evaporator and using a similar milling procedure to form the hole.

**Transmission measurements.** Normalized transmission of the different hole arrays have been measured by using light from a super continuum laser (SuperK Extreme by NKT Photonics) filtered through a monochromator, and sent at normal incidence on the sample.

**Optical setup.** The pump photon source is a Coherent laser diode emitting linearly polarized photons at 406 nm with an optical output power up to 100 mW. SPDC process is achieved with BiBO crystal. Single photon detection is performed by two  $\tau$ -SPADs Single Photon Counting Modules by PicoQuant.

## References and Notes

1. E. Knill, R. Laflamme, G.J. Milburn, A Scheme for Efficient Quantum Computation with Linear Optics. *Nature* **409**, 46-52 (2001).
2. J. Sun, E. Timurdogan, A. Yaacobi, E.S. Hosseini, M. R. Watts, Large-Scale Nanophotonic Phased Array. *Nature* **493**, 195–199 (2013).
3. R. H. Ritchie, Plasma losses by fast electrons in thin films. *Physical Review*, **106**(5), 874 (1957).
4. R. Alvarez-Puebla, B. Cui, J. P. Bravo-Vasquez, T. Veres, H. Fenniri, Nanoimprinted SERS-active substrates with tunable surface plasmon resonances. *The Journal of Physical Chemistry C* **111**(18), 6720-6723 (2007).
5. J. Homola, Surface plasmon resonance sensors for detection of chemical and biological species. *Chemical reviews* **108**(2), 462-493 (2008).
6. T. Taubner, D. Korobkin, Y. Urzhumov, G. Shvets, R. Hillenbrand, Near-field microscopy through a SiC superlens. *Science* **313**, 1595 (2006).
7. J. N. Farahani, D. W. Pohl, H.-J. Eisler, B. Hecht. Single quantum dot coupled to a scanning optical antenna: a tunable superemitter. *Phys. Rev. Lett.* **95**, 17402 (2005).
8. J. Dintinger, S. Klein, F. Bustos, W. L. Barnes, T. W. Ebbesen. Strong coupling between surface plasmon-polaritons and organic molecules in subwavelength hole arrays. *Physical Review B* **71**(3), 035424 (2005).
9. D. E. Chang, A. S. Sørensen, P. R. Hemmer, M. D. Lukin. Strong coupling of single emitters to surface plasmons. *Physical Review B*, **76**(3), 035420 (2007).
10. M.-C. Dheur, E. Devaux, T. W. Ebbesen, A. Baron, J.-C. Rodier, J.-P. Hugonin, J.-J. Greffet, G. Messin, F. Marquier, Single-plasmon interferences. *Science advances* **2**(3), e1501574 (2016).
11. R. Kolesov, B. Grotz, G. Balasubramanian, R. J. Stöhr, A. A. Nicolet, P. R. Hemmer, F. Jelezko, J. Wrachtrup, Wave–particle duality of single surface plasmon polaritons. *Nature Physics* **5**(7), 470 (2009).
12. J. S. Fakonas, H. Lee, Y. A. Kelaita, H. A. Atwater, Two-plasmon quantum interference. *Nature Photonics* **8**(4), 317 (2014).

13. G. Di Martino, Y. Sonnefraud, M.S. Tame, S. Kéna-Cohen, F. Dieleman, Ş. K. Özdemir, M. S. Kim, S. A. Maier, Observation of quantum interference in the plasmonic Hong-Ou-Mandel effect. *Physical Review Applied* **1**(3), 034004 (2014).
14. B. Vest, M.-C. Dheur, É. Devaux, A. Baron, E. Rousseau, J.-P. Hugonin, J.-J. Greffet, G. Messin, F. Marquier. Anti-coalescence of bosons on a lossy beam splitter. *Science* **356**(6345), 1373-1376 (2017).
15. E. Altewischer, M. P. van Exter, J. P. Woerdman, Plasmon-Assisted Transmission of Entangled Photons. *Nature* **418**, 304-306 (2002).
16. M.-C. Dheur, B. Vest, É. Devaux, A. Baron, J.-P. Hugonin, J.-J. Greffet, G. Messin, F. Marquier, Remote preparation of single-plasmon states. *Physical Review B*, **96**(4), 045432 (2017).
17. J. S. Fakonas, A. Mitskovets, H. A. Atwater, Path-Entanglement of Surface Plasmons. *New Journal of Physics* **17**, 023002 (2015).
18. S. G. Dlamini, J. T. Francis, X. Zhang, Ş. K. Özdemir, S. N. Chormaic, F. Petruccione, M. S. Tame, Probing decoherence in plasmonic waveguides in the quantum regime. *Physical Review Applied*, **9**(2), 024003 (2018).
19. T. W. Ebbesen, H. J. Lezec, H. F. Ghaemi, T. Thio, P. A. Wolff, Extraordinary optical transmission through sub-wavelength hole arrays. *Nature* **391**, 667 (1998).
20. R. Rangarajan, M. Goggin, P. Kwiat, Optimizing type-I polarization-entangled photons. *Optics Express* **17**(21), 18920-18933 (2009).
21. J. Bell, On The Problem of Hidden Variables in Quantum Mechanics. *Reviews of Modern Physics* **38**(3), 447-452 (1966).
22. J. Clauser, M. Horne, A. Shimony, R. Holt, Proposed Experiment to Test Local Hidden-Variable Theories. *Physical Review Letters* **23**(15), 880-884 (1969).
23. K. Puech, F. Z. Henari, W. J. Blau, D. Duff, G. Schmid, Investigation of the ultrafast dephasing time of gold nanoparticles using incoherent light. *Chemical Physics Letters* **247**, 13-17 (1995).
24. E. Palik, *Handbook of optical constants* (Academic press, 1998), vol. 3.
25. P. B. Johnson, R. W. Christy, Optical constants of the noble metals. *Physical review B*, **6**(12), 4370 (1972).

## Acknowledgments

**General.** We acknowledge Yousif Kelaita, Artur Davoyan, Ruzan Sokhoyan, Ragip Pala, Dagny Fleishman, Zachary Aitken, Sunita Darbe for help with equipment training and scientific advice.

**Funding.** This work was supported by the Air Force Office of Scientific Research under grant number FA9550-16-1-0019.

**Author contributions:** Y.S.T., J.S.F. and H.A.A. proposed the original idea. Y.S.T. realized all experiments and data analysis. B. V. helped in discussion. Y.S.T., B.V., H.A.A. wrote the paper, and all authors discussed and revised the manuscript.

**Competing interests:** The authors declare no competing interests.

**Data and materials availability:** All data needed to evaluate the conclusions of this study are presented in the paper. Additional data related to this study maybe requested from H.A.A. (haa@caltech.edu).

## Figures and Tables

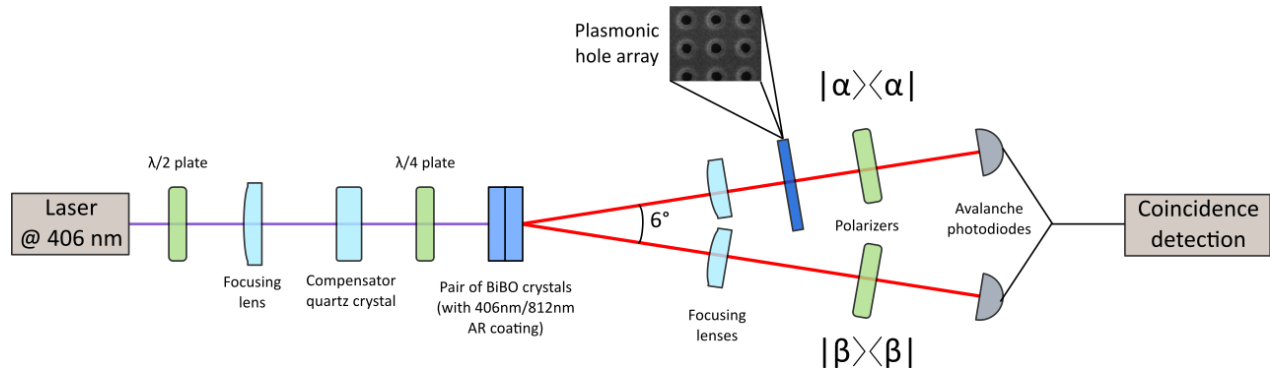


**Figure 1. Experimental setup for the measurement of polarization-entanglement preservation.** Pump photons at 406 nm are sent toward a pair of BiBO crystals and generate pairs of polarization entangled photons that propagate along two separate path. Along the upper path, we can insert a metallic hole array, and measure the transmission of the entangled light that has been coupled to plasmons.

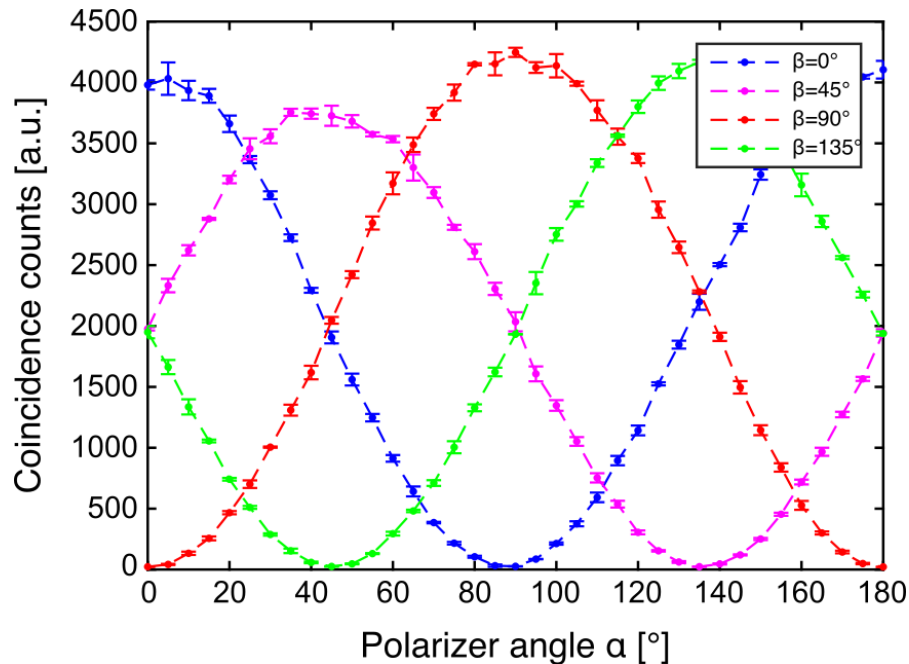


**Figure 2. Calibration of the setup, and entanglement between produced pairs of photons.** Number of coincidence counts as a function of polarizers angles without plasmonic sample (solid lines are fits to cosine).

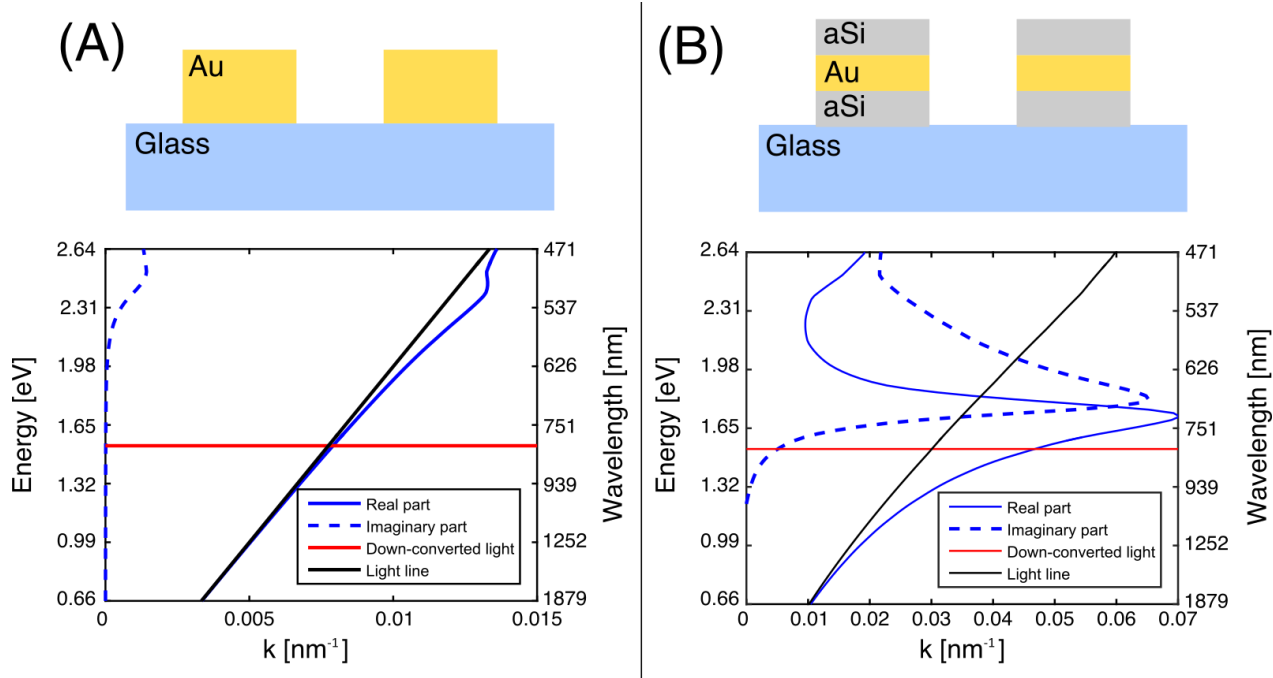


**Figure 3. Plasmonic hole array designs in our experiments.** (A) cross-sectional schematic and dispersion relation of elliptical hole arrays for SPPs supported at the gold/glass interface. At the wavelength of the down-converted photons (812 nm), the dispersion is ‘photon-like’, i.e., linear and very close to the light line; (B) cross-sectional schematic and dispersion relation of circular hole arrays for SPPs supported in the silicon/gold/silicon structure, which exhibits strongly nonlinear dispersion at 812 nm.

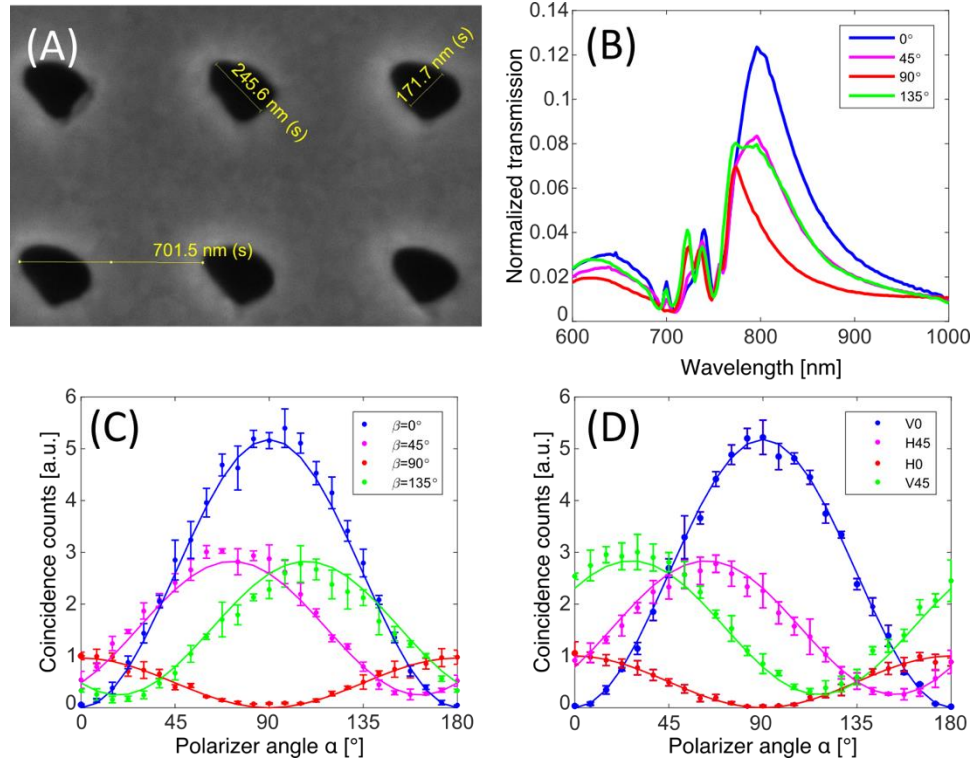


**Figure 4. Study of entanglement preservation with the elliptical hole array.** Elliptical hole array used to study the influence of hole geometry on the preservation of photon entanglement: **(A)** SEM image, where the orientation of the minor and major axis can be seen oriented at  $\pm 45^\circ$ ; **(B)** transmission factor of the device for different polarizations of incident light. The holes have no rotation symmetry anymore, so that the transmission maximum varies between 12.5 % for horizontally polarized light and 7% for vertically polarized light. **(C)&(D)** Normalized number of coincidence counts as a function of polarizer angles in the presence of an elliptical plasmonic hole array (solid line represents fit to the full model) in two configurations : **(C)** With entangled photons and for different fixed directions of the polarizer beta; **(D)** With classical light and similar choice for beta. The plots with  $b = 45^\circ$  and  $b = 135^\circ$  show a similar decrease in visibility in both configurations, indicating that this results from a purely classical effect.

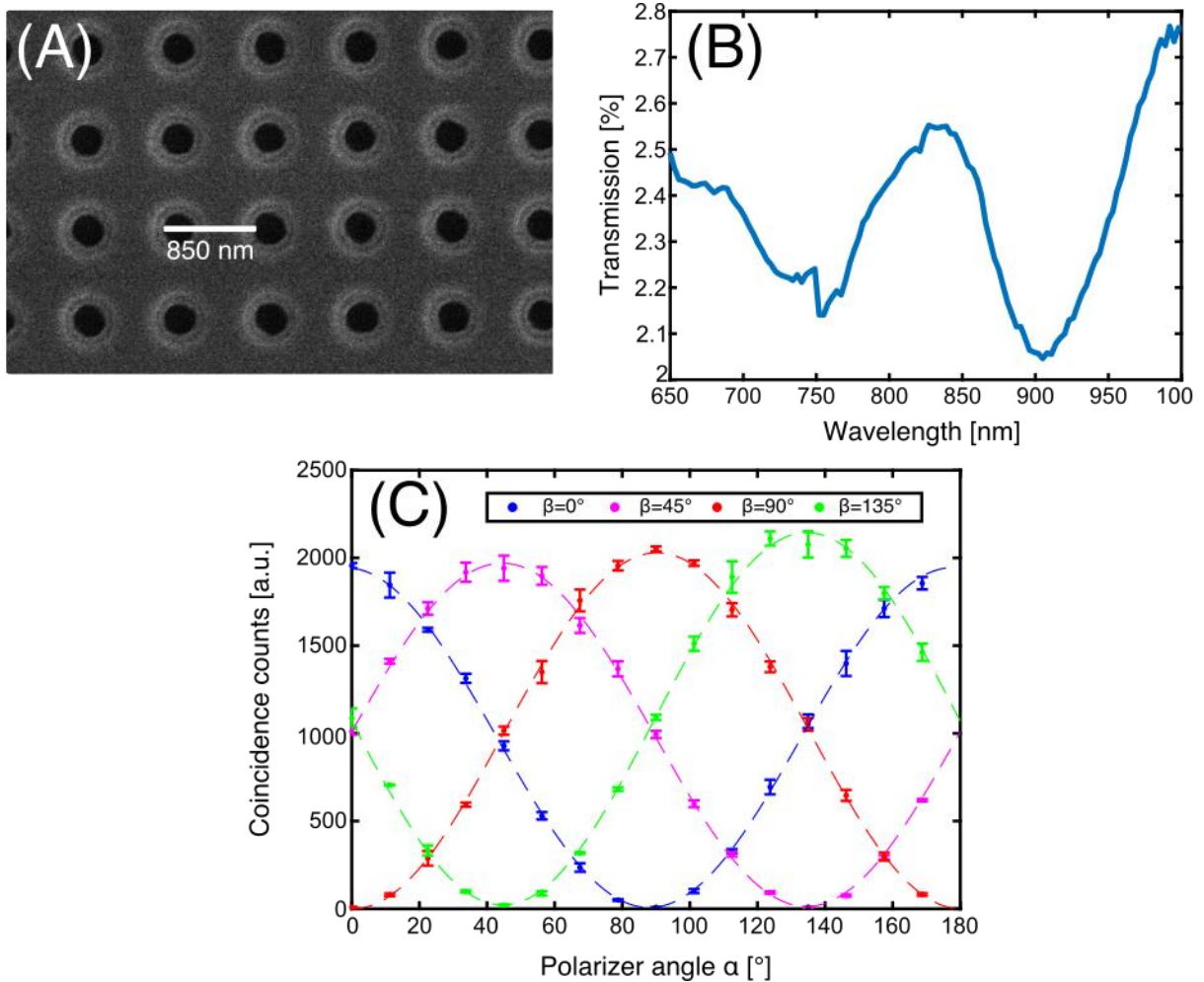


**Figure 5. Hole array with highly-dispersive plasmons.** (A) SEM image of the sample. The period of the 2D array is 850 nm. The different material species experience different milling rate that slightly affect the shape of the holes perimeter. (B) Transmission spectrum of the hole array. The holes being circular, there is no polarization dependence. The broadening of the transmission feature around 810 nm can be attributed to the unperfect shape of the holes. Note that the plasmons experience a higher absorption than in the previous experiment. (C) Number of coincidence counts as a function of polarizer angles in the presence of a hole array with highly-dispersive regime (solid lines are fits to cosine). Whatever the choice of beta is and even when placed at  $45^\circ$  or  $135^\circ$ , the visibility of quantum interference remains almost equal to one.

## Supplementary Information for :

### Quantum Coherence is Preserved in Extremely Dispersive Plasmonic Media

Yury S. Tokpanov<sup>1</sup>, James S. Fakonas<sup>1</sup>, Benjamin Vest<sup>1</sup>, and Harry A. Atwater<sup>1\*</sup>

#### Affiliations

<sup>1</sup>Thomas J. Watson Laboratories of Applied Physics, California Institute of Technology, Pasadena, California 91125.

#### Non-linear dispersion regime of the fabricated structures

We present here further analysis that we performed to confirm that the fabricated hole arrays display characteristics that match the numerical simulations performed for the design of the structure.

The direct comparison of the transmission spectrum at normal incidence of a single structure with the simulated data is made difficult by the overall extreme sensitivity of surface plasmons to geometric defects and roughness of the different layers (intrinsically related to the limits of the fabrication process), that were not included in the numerical model of the structure (performed using only perfectly flat layers). These effects result in a broadening of the transmission peaks in the experimental data, that complicate the identification of the different resonances.

In order to overcome this difficulty, we fabricated a set of hole arrays with different periodicity ranging from 600 nm to 1000 nm, following the same fabrication procedures (resulting in the same films thicknesses and hole diameters). The period of the structures defines the wavevectors of plasmons that can couple to the structures. Overall, and thanks to the reproducibility of the fabrication processes, the acquisition of transmission spectra at normal incidence for these different structures can be seen as an indirect measurement of the dispersion relation of the structure. The next step of our approach consists in comparing these experimental transmission spectra of the different hole array structures with the analytical dispersion relation displayed on Figure 3, and to check if the evolution of their respective characteristics (in practice, evolution and spectral shift of the resonance maxima) are compatible with each other.

Figure S1 displays an interpolation of a set of transmission spectra obtained experimentally for the nine different structures (color map). The operating point of our main experiment, with a structure of periodicity 850 nm and a plasmon energy around 1.52 eV, is marked with a black cross. The map displays different branches, i.e. different sets of plasmon energies and wavevectors that fulfill a resonant condition, all excited in parallel when performing our experiment, and corresponding to different folded portions of the dispersion relation of the structure.

In first approximation, the resonance condition fulfilled by plasmons propagating in the structure can be expressed as:

$$\sqrt{2}p = d + 2\pi n/k \quad (1)$$

where  $p$  is the period of the structure,  $d$  is the hole diameter,  $k$  is the plasmon momentum and  $n$  is an integer. The factor  $\sqrt{2}$  takes into account the fact, that in our experiment hole array plasmon eigenmodes propagate along diagonal directions. SEM images and measurements show that two values must be considered for the holes diameter. The diameter of the holes in the upper aSi layer is  $d=430$  nm and is associated to plasmons propagating along the upper aSi-gold interface. The etching process produced smaller holes in the lower aSi layer, with a diameter  $d=300$ nm, this value being this time associated to plasmons propagating along the lower gold-aSi interface. Using the analytical

dispersion relation of Fig. 3 to relate the plasmon momentum  $k$  and the plasmon energy, we plot the relation (1) on Fig S1(A) for different values of  $n$  and different values of the hole diameter. We see that we have great agreement between our experimental data and the model of (1) for different branches, and in particular for the plasmon resonance that we exploit in our experiments (branch labeled "P0" of the colormap including the black cross) when considering  $n=6$  and  $d=300\text{nm}$  for the bottom plasmon (blue solid line) and  $n=5$ ,  $d=430\text{nm}$  for the top plasmon (red solid line). We emphasize that, while we can in theory expect two different resonances for the two plasmons propagating in the structure, or in other words two sets of branches, in practice, both are significantly broadened and merge into each other. It is not possible to resolve them separately and "P0" displays only one local transmission maximum although it contains the contribution of both top-propagating plasmons and bottom-propagating plasmons.

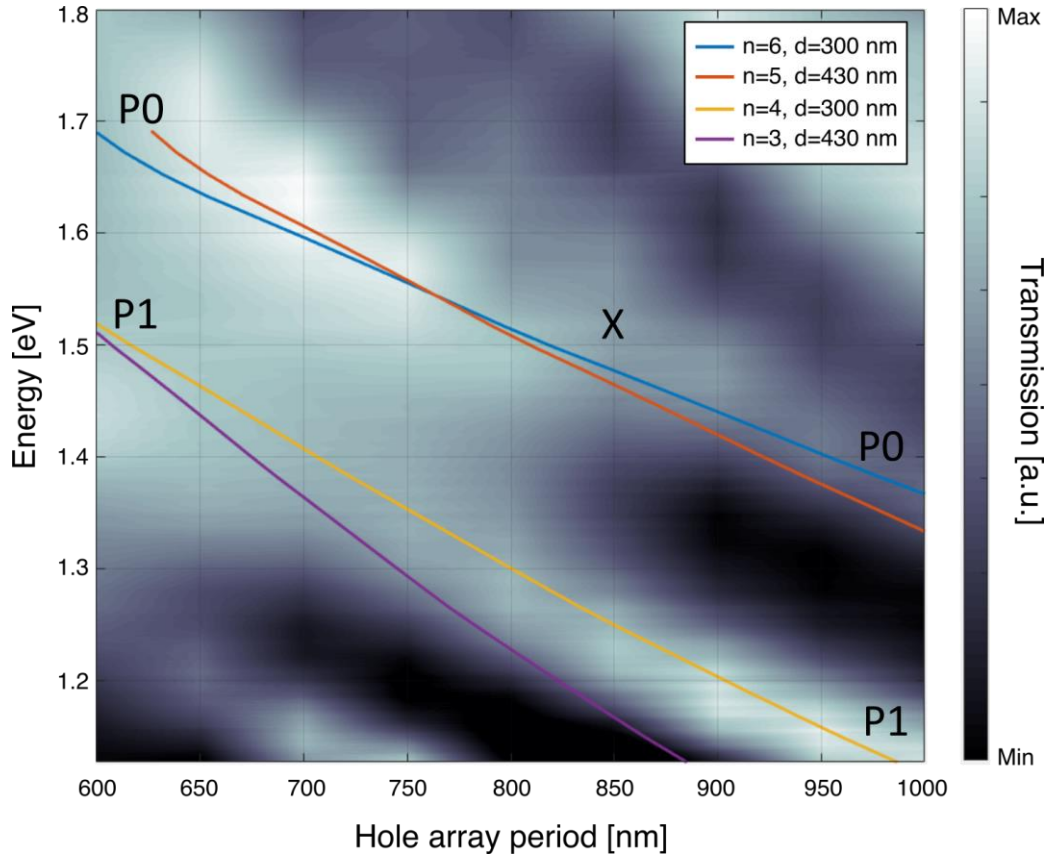


**Figure S1. Investigation of the evolution of the transmission resonances for various structures.** The transmission spectra at normal incidence of nine different hole array structures, with periods ranging from 600 nm to 1000 nm have been experimentally measured. The transmission amplitude is displayed as a color map, and as a function of both the energy (vertical axis) and of the periodicity of the hole array (horizontal axis). Experimental data have been interpolated between the nine sets of data points. The different white branches displayed on the colormap correspond to transmission resonances. The branch corresponding to the plasmon resonance exploited in the main experiment is labeled as P0 and the operating point of the experiment (structure periodicity of 850 nm, plasmon resonance at 812 nm) is marked with a black X. Another branch of plasmon resonance at lower energies is identified as P1. These branches were fitted using relation (1) for different sets of parameters (solid color lines). For both P0 and P1 agreement between experimental data and model is good and allows us to determine the plasmon wavevectors at resonance.

The parameters  $n$  and  $d$  allow us to identify the proper fraction of the dispersion relation that has to be compared with our transmission measurements. Using relation (1) and the parameters  $n=6$  and  $d=300\text{nm}$ , we now plot on Fig. S2 our experimental transmission measurements as a function of plasmon energy and  $k = \frac{2\pi n}{\sqrt{2}p-d}$ , the wavevector corresponding to the excitation of the plasmons belonging to P0, and we superimpose on the same plot the dispersion

relation of Fig 3. This choice of plot highlights the agreement between or experimental data and the initial numerical design of the structure.

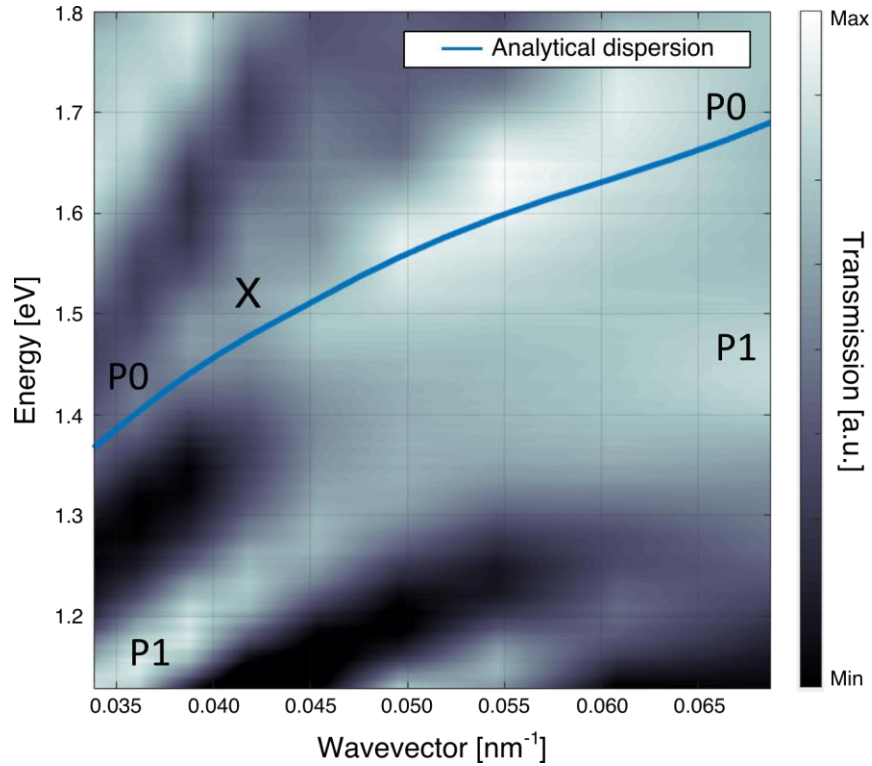


**Figure S2. Comparison of the analytical dispersion relation with the transmission measurements.** The colormap of Fig S1 is represented this time as a function of the wavevector, using the conversion between periodicity of the structures and resonant wavevectors given by relation (1) with  $n=6$  and  $d=300\text{nm}$ . The two branches P0 and P1 are identified on the plot, as same as the operating point of the main experiment marked with a black X. P0 is well fitted by a segment of the dispersion relation that corresponds to a non-linear highly-dispersive regime for the plasmons (blue solid line), and the position of the operating point is in agreement with the initial design of the experiment.

We finally check the robustness of our model by unfolding further the data of the transmission spectra and comparing them with the analytical dispersion relation on a larger wavevector scale. We consider, for each of the nine transmission spectra obtained with the nine experimentally characterized structures (vertical cross sections of figure S1), the wavelengths of the two local transmission maxima corresponding to both branches P0 and P1. As previously discussed, each one of these transmission peaks merges the contribution of the two plasmons propagating in the structure, either along the top or along the bottom gold-aSi interface. On Fig S3, we compare our experimental measurement of the different transmission maxima for the different structures with the analytical dispersion relation (black solid line). Each transmission maximum that was experimentally measured in the different spectra is represented as two data points placed at the same plasmon energy, but at the two different wavevectors corresponding to the top plasmon and the bottom plasmon. The values of the two plasmon wavevectors were derived using the relation (1) with the two sets of parameters ( $n,d$ ) associated to P0 or P1. We can see that this unfolding procedure shows great agreement between our experimental spectra and the dispersion relation for the two major resonance branches that could be observed.

We can conclude that, taking into account geometrical defects and possible small discrepancy in optical constants between experimental and literature values used in simulations, the experimental dispersion relation is compatible with our analytical model, and that the chosen operating point at 812nm for the structure with a periodicity of 850 nm corresponds with a surface plasmon following the intended resonance far from the light line, in the highly-dispersive regime.

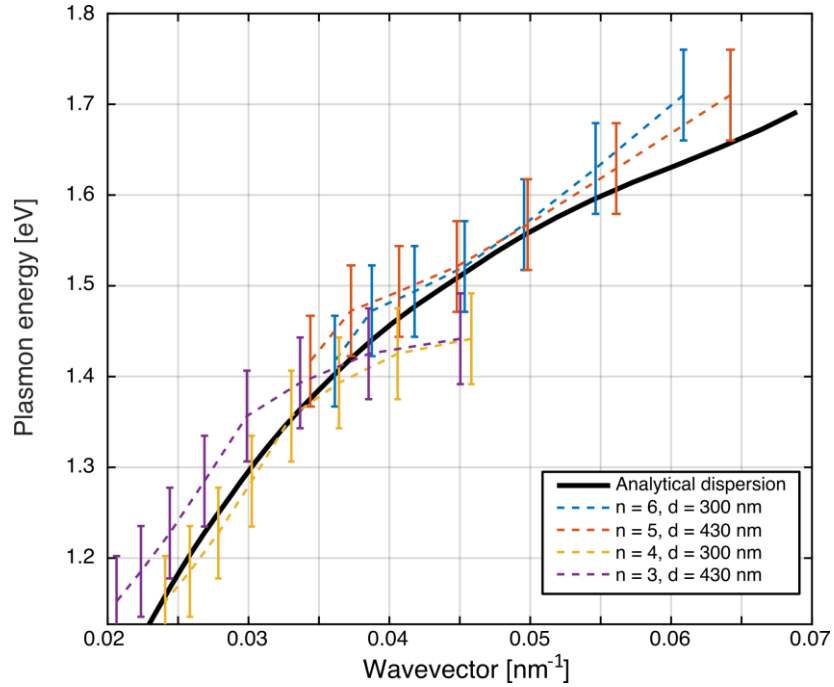


**Figure S3. Unfolding the transmission spectra to measure indirectly the dispersion relation.** We compare the analytical dispersion relation (black solid line) of the structure with the position of the local transmission maxima measured experimentally with structures of various periodicities (vertical cross sections of fig S1). For each measured transmission maximum, two values of associated wavevector are derived, by using (1) with two sets of parameters. If the transmission maximum belongs to the branch P0, the two wavevectors values are calculated using  $n=6$ ,  $d=300\text{nm}$  (dashed blue line) or  $n=5$ ,  $d=430\text{ nm}$  (dashed red line). If the transmission maximum belongs to the branch P1, the two wavevectors values are calculated using  $n=4$ ,  $d=300\text{nm}$  (dashed yellow line) or  $n=3$ ,  $d=430\text{ nm}$  (dashed purple line). This shows that experimental transmission spectra are in great agreement with the expected dispersion relation.